

Numerical Heat Transfer, Part B: Fundamentals

An International Journal of Computation and Methodology

ISSN: 1040-7790 (Print) 1521-0626 (Online) Journal homepage: <https://www.tandfonline.com/loi/unhb20>

A volume of fluid method algorithm for simulation of surface tension dominant two-phase flows

Z. H. Gu, H. L. Wen, Yuan Yao & C. H. Yu

To cite this article: Z. H. Gu, H. L. Wen, Yuan Yao & C. H. Yu (2019) A volume of fluid method algorithm for simulation of surface tension dominant two-phase flows, Numerical Heat Transfer, Part B: Fundamentals, 76:1, 1-17, DOI: [10.1080/10407790.2019.1642048](https://doi.org/10.1080/10407790.2019.1642048)

To link to this article: <https://doi.org/10.1080/10407790.2019.1642048>



Published online: 22 Jul 2019.



Submit your article to this journal [↗](#)



Article views: 12



View Crossmark data [↗](#)



A volume of fluid method algorithm for simulation of surface tension dominant two-phase flows

Z. H. Gu^a, H. L. Wen^b, Yuan Yao^a, and C. H. Yu^c

^aCollege of Civil Engineering and Architecture, Zhejiang University, Hangzhou, P.R. China; ^bDepartment of Engineering Science and Ocean Engineering, National Taiwan University, Taipei, P.R. China; ^cState Key Lab of Hydraulics and Mountain River Engineering, Sichuan University, Chengdu, P.R. China

ABSTRACT

In this article, a two-phase flow algorithm that uses an explicit Adams–Bashforth scheme coupled with volume of fluid (VOF) method in a uniform staggered Cartesian grid for surface tension dominant simulation is presented. The interface reconstruction procedure is implemented using the Weighed Linear Interface Calculation (WLIC) algorithm. The level set (LS) function instead of VOF function is adopted for calculation of not only the interface normal vectors in the WLIC algorithm but also the surface tension terms in the Navier–Stokes equations. This VOF method is compared with LS method and other experiment results in the literature for vortex deforming, milk crown, droplet impacting into deep liquid pool and bubble bursting at a free surface problems to show whether mass can be well conserved and breaking and merging phenomena can be accurately simulated.



ARTICLE HISTORY

Received 4 April 2019
Accepted 5 July 2019

1. Introduction

Two-phase flow problems taking into account surface tension force have wide applications in both scientific and industrial fields, and are closely related to physical phenomena such as particle motion in droplet evaporation [1], bubble condensation in subcooled liquid [2], leaky dielectric droplet [3], droplet impacting onto spheres [4], and droplet splashing on substrate [5, 6]. Numerical simulation of incompressible two-phase flow remains a challenge due to the difficulties in the calculation of interface breaking or merging and surface tension force near the interface. In addition, improper numerical methods can cause significant mass loss [7].

Interface tracking and capturing methods in fixed grids have been utilized to accurately and efficiently obtain solutions to resolve the above problems of interfacial flows [8, 9]. In interface tracking methods, the interface is tracked by using a moving surface mesh, and the interface deformation is modeled by adopting a computationally expensive re-meshing procedure. Typical examples of this kind of method include that of Unverdi and Tryggvason [10], and extensive studies by Han and Tryggvason [11]. Interface capturing methods have an excellent advantage of capturing strong topological changes with relative ease such as break up and merger of bubbles or droplets [12]. Frequently used interface capturing methods include volume of fluid (VOF) [13–18] and level set (LS) [19–24], both of which use a scalar indicator function to distinguish two phases in the whole computational domain.

CONTACT C. H. Yu  chyu@zju.edu.cn  State Key Lab of Hydraulics and Mountain River Engineering, Sichuan University, Chengdu, P.R. China

Color versions of one or more of the figures in the article can be found online at www.tandfonline.com/unhb.

NOMENCLATURE

| | | | |
|---------------------|-----------------------------|-------------------|-------------------------|
| \mathbf{u} | velocity field | $\bar{S}(\phi_0)$ | smoothed sign function |
| $\delta(\phi)$ | Dirac delta function | Δx | grid cell size |
| $\mathcal{H}(\phi)$ | smoothed Heaviside function | X | characteristic function |
| \mathbf{g} | gravitational acceleration | p | pressure |
| $\kappa(\phi)$ | curvature of the interface | M | viscosity |
| ρ | density | | |
| C | volume of fluid function | | |

The LS method was proposed by Sussman et al. [25], which can effectively simulate incompressible two-phase flows when surface tension force needs to be considered. This method adopts a continuous function ϕ , defined as the signed distance to the interface and termed as the LS function, to distinguish the two phases separated by the interface. ϕ is positive in the liquid, zero on the interface, and negative in the gas. Advection and re-initialization procedures are commonly employed [26–28] in the LS method. The resolved velocity field is used to solve the advection equation to obtain the evolution of the interface. A re-initialization procedure is then performed to ensure the advected LS function remains a signed distance function. The advantage of the LS method lies in the smoothness of the LS function which makes it easy to calculate the interface curvature [29–31]. However, LS methods may result in significant mass loss because the zero LS may deviate from the real position during the simulation when solving the advection and re-initialization equations. A high-resolution scheme known as weighted essentially non-oscillatory (WENO) reduces mass loss by solving the advection equation in a Cartesian mesh, and is used to simulate a surface tension dominant droplet impacting on a plate [32].

Different from the LS method which uses a continuous distance function, the VOF method utilizes a discontinuous volume fraction function which refers to the volume fraction occupied by the liquid within each cell, with a value between 0 and 1. The VOF function is discontinuous across the interface, which makes it quite difficult to calculate interface curvature. There have emerged two kinds of VOF methods for advection of the volume fraction over the past several decades. One is the algebraic VOF method, where the VOF field is transported by a convective term using discretization methods. However, if a high-resolution advection scheme is used to approximate the convective term in the VOF transport equation, interface smearing which reduces accuracy on the interface can be evident [33]. Xiao et al. have further developed an algebraic VOF method to resolve smearing problems by using a hyperbolic tangent function to compute the numerical flux. This method, known as THINC (tangent of hyperbola for interface capturing), suppresses oscillations without the need of an extra geometric reconstruction. This method is particularly amenable to numerical simulation due to the relative ease of operating parameters in hyperbolic tangent function [33]. Another VOF method which defines and reconstructs the interface location within a cell using the volume fraction α and interface normal $\nabla\alpha$ can be used to overcome this problem. There have been numerous studies on interface reconstruction. For example, simple line interface calculation (SLIC) proposed by Noh and Woodward [34], piecewise linear interface calculation (PLIC) proposed by Youngs [35, 36], and weighted line interface calculation (WLIC) which adjusts the SLIC method with a weight related to the geometry at the interface [37].

By combining the mass conservation of VOF and the continuous function description of LS, the coupled level set and volume of fluid (CLSVOF) method has been utilized on study of surface tension dominant two-phase flows [38–43]. In these two-way coupling methods (CLSVOF), initialization and correction are carried out on the whole field, LS function and VOF function. However, they are considerably complicated and computationally expensive compared to VOF

and LS methods [44]. Sun and Tao [45] developed a coupled VOF and LS method for simulating incompressible two-phase flows. In their method, only the advection equation of the volume fraction α needs to be solved, while the LS function is directly calculated from a simple iterative geometric operation, making this method even simpler than the CLSVOF method [46, 47].

In our method, a transport equation is solved only for VOF by using the THINC/WLIC scheme, and the need for solving the transport equation for the LS method is obviated. Instead, a LS is constructed from the interface (defined as the VOF = 0.5 isosurface). This allows more accurate calculations of the surface curvature using the LS. In Section 2, the governing equations for the two fluids and the VOF method are presented. Section 3 describes the proposed solution algorithm. In Section 4, vortex deforming, milk crown, droplet impacting into deep liquid pool, and bubble bursting at a free surface problems are investigated to confirm the integrity of the proposed two-phase flow model. Conclusions are drawn in Section 5.

2. Numerical model

2.1. Governing equations

We consider the following continuity, momentum, and VOF equations for two immiscible and incompressible flows

$$\nabla \cdot \mathbf{u} = 0, \quad (1)$$

$$\rho \left(\frac{\partial \mathbf{u}}{\partial t} + \nabla \cdot \mathbf{u}\mathbf{u} \right) = -\nabla p + \nabla \cdot [\mu(\nabla \mathbf{u} + \nabla \mathbf{u}^T)] + \mathbf{F}_B, \quad (2)$$

$$\frac{\partial C}{\partial t} + \nabla \cdot (\mathbf{u}C) - C\nabla \cdot \mathbf{u} = 0, \quad (3)$$

where \mathbf{u} is the velocity vector, p is the pressure, and C is the VOF function. The body force term \mathbf{F}_B on the right-hand side of Eq. (2) contains the gravitational force $\rho\mathbf{g}$ and surface tension force \mathbf{f}_{sf} terms. The surface tension force term can be calculated based on the standard continuum surface force (CSF) model [48]

$$\mathbf{f}_{sf} = \sigma\kappa(\phi)\delta(\phi)\nabla\phi, \quad (4)$$

where ϕ is the LS function and κ is the free surface curvature calculated by

$$\begin{aligned} \kappa(\phi) &= -\nabla \cdot \left(\frac{\nabla\phi}{|\nabla\phi|} \right) \\ &= -(\phi_x^2\phi_{yy} - 2\phi_x\phi_y\phi_{xy} + \phi_y^2\phi_{xx} + \phi_x^2\phi_{zz} - 2\phi_x\phi_z\phi_{xz} + \phi_z^2\phi_{xx} \\ &\quad + \phi_y^2\phi_{zz} - 2\phi_y\phi_z\phi_{yz} + \phi_z^2\phi_{yy})/(\phi_x^2 + \phi_y^2 + \phi_z^2)^{\frac{3}{2}}. \end{aligned} \quad (5)$$

However, the implementation of the standard CSF model cannot reduce spurious currents for surface tension dominant two-phase flows such as droplet splashing and bubble rising problems [49]. Instead, the density-scaled CSF model proposed by Yokoi [49] which avoids spurious currents will be adopted in this study, where the following surface tension force term is specified:

$$\mathbf{f}_{sf} = \sigma\kappa(\phi)\delta^{scaling}(\phi)\nabla\phi, \quad (6)$$

where σ is the surface tension coefficient of liquid in gas, and

$$\delta^{scaling}(\phi) = 2\mathcal{H}(\phi)\delta(\phi). \quad (7)$$

In Eq. (7), $\mathcal{H}(\phi)$ is a continuous function named smeared Heaviside function, whose value is zero for negative argument and one for positive argument

$$\mathcal{H}(\phi) = \begin{cases} 0 & ; \text{ if } \phi < -\varepsilon, \\ \frac{1}{2} \left[1 + \frac{\phi}{\varepsilon} + \frac{1}{\pi} \sin \left(\frac{\pi\phi}{\varepsilon} \right) \right] & ; \text{ if } |\phi| \leq \varepsilon, \\ 1 & ; \text{ if } \phi > \varepsilon, \end{cases} \quad (8)$$

with $\varepsilon = 1.5\Delta x$ and Δx being the mesh cell. It is noted that the delta function $\delta(\phi)$ in Eq. (7) can be obtained from the following equation

$$\delta(\phi) = \frac{d\mathcal{H}(\phi)}{d\phi} = \begin{cases} \frac{1}{2\varepsilon} \left(1 + \cos \left(\frac{\pi\phi}{\varepsilon} \right) \right) & ; \text{ if } |\phi| < \varepsilon; \\ 0 & ; \text{ otherwise.} \end{cases} \quad (9)$$

In Eq. (2), the two material properties, namely, density ρ and dynamic viscosity μ , are given as follows:

$$\rho = \rho_G + (\rho_L - \rho_G) C, \quad (10)$$

$$\mu = \mu_G + (\mu_L - \mu_G) C, \quad (11)$$

where ρ_G and ρ_L are the density in gas and liquid, respectively. C in Eqs. (10) and (11) is the volume fraction defined as

$$C_{ij} = \frac{1}{\Delta x \Delta y} \int_0^{\Delta x} \int_0^{\Delta y} \chi(x, y) dx dy \quad (12)$$

with

$$\chi(x, y) = \begin{cases} 1; & \text{for } (x, y) \in \text{the liquid,} \\ -1; & \text{for } (x, y) \in \text{the gas.} \end{cases} \quad (13)$$

Because of the diffuse yet bounded solution derived from low-order convective schemes and conservative high-resolution schemes, smearing may occur in interfacial cells after advection of the VOF field, as shown in Eqs. (14) and (15). This means that numerical oscillations can be effectively prevented by using a conservative high-resolution scheme with a well-designed flux limiter or slope limiter. However, the initial jump in the density function will be smeared by this kind of scheme, thanks to its inherent numerical diffusions. Higher order schemes can also be used, but when they are applied in scalar fields with sharp interfaces, the results may become unstable and unbounded in the vicinity of the interface. In this study, we use the THINC/WLIC scheme described in Section 2.3 to simulate the time-evolving volume fraction field.

2.2. VOF advection

The VOF advection equation in this numerical model is discretized by utilizing the dimensional splitting algorithm

$$C_{i,j}^* = C_{i,j}^n - \frac{F_{x,i+1/2,j}^n - F_{x,i-1/2,j}^n}{\Delta x} - C_{i,j}^n \frac{u_{x,i+1/2,j} - u_{x,i-1/2,j}}{\Delta x} \Delta t, \quad (14)$$

$$C_{i,j}^{n+1} = C_{i,j}^* - \frac{F_{y,i,j+1/2}^* - F_{y,i,j-1/2}^*}{\Delta y} - C_{i,j}^* \frac{u_{y,i,j+1/2} - u_{y,i,j-1/2}}{\Delta y} \Delta t, \quad (15)$$

in which the terms $F_{x,i+1/2,j}$ and $F_{y,i,j+1/2}$ denote the flux given below

$$F_{x,i+1/2,j} = - \int_{y_{ij-1/2}}^{y_{ij+1/2}} \int_{x_{i+1/2,j}}^{x_{i+1/2,j} - u_{x,i+1/2,j} \Delta t} \chi_{is,j}(x, y) dx dy, \quad (16)$$

$$F_{y,i,j+1/2} = - \int_{y_{i,j+1/2}}^{y_{i,j+1/2} - u_{y,i,j+1/2}\Delta t} \int_{x_{i-1/2,j}}^{x_{i+1/2,j}} \chi_{i,js}(x, y) dx dy. \quad (17)$$

The subscript is and js in Eqs. (16) and (17) are

$$is = \begin{cases} i; & \text{if } u_{x,i+1/2,j} \geq 0, \\ i + 1; & \text{if } u_{x,i+1/2,j} < 0, \end{cases} \quad (18)$$

and

$$js = \begin{cases} j; & \text{if } u_{y,i,j+1/2} \geq 0, \\ j + 1; & \text{if } u_{y,i,j+1/2} < 0. \end{cases} \quad (19)$$

2.3. THINC/WLIC method

In order to improve the transport of fluid interfaces involving geometric interface reconstruction, the WLIC method proposed by Yokoi [37] is used. We present below the employed characteristic function χ shown in Eq. (20), which consists of the vertical interface $\chi_{x,i,j}(x, y)$ and horizontal interface $\chi_{y,i,j}(x, y)$

$$\chi_{i,j}(x, y) = \omega_{x,i,j}(\mathbf{n}_{i,j})\chi_{x,i,j}(x, y) + \omega_{y,i,j}(\mathbf{n}_{i,j})\chi_{y,i,j}(x, y), \quad (20)$$

with weights $\omega_{x,i,j}$ and $\omega_{y,i,j}$. The weights are defined as

$$\omega_{x,i,j} = \frac{|n_{x,i,j}|}{|n_{x,i,j}| + |n_{y,i,j}|}, \quad (21)$$

$$\omega_{y,i,j} = \frac{|n_{y,i,j}|}{|n_{x,i,j}| + |n_{y,i,j}|}, \quad (22)$$

where $n_{x,i,j}$ and $n_{y,i,j}$ are x component and y component of the surface normal. The surface normals can be obtained from the VOF function [37]. However, this may lead to inaccurate solutions near the interface where the VOF function's spatial derivatives are discontinuous.

To improve the calculation of surface normals, the representative LS function (or continuous signed distance function) instead of VOF function in the above surface normal term, which is given by $\mathbf{n}_{i,j} = \frac{(\nabla\phi)_{i,j}}{|\nabla\phi|_{i,j}}$, will be approximated by the second-order central difference scheme. For example,

$$(\nabla\phi)_{i,j} = \frac{\phi_{i+1,j} - \phi_{i-1,j}}{2\Delta x} \hat{x} + \frac{\phi_{i,j+1} - \phi_{i,j-1}}{2\Delta y} \hat{y}. \quad (23)$$

To compute the characteristic functions of the vertical interface in Eq. (20), the THINC scheme is employed. The characteristic function can be represented by the piecewise hyperbolic tangent function, which is given below:

$$\chi_{x,i} = \frac{1}{2} \left(1 + \alpha \tanh \left(\beta \left(\frac{x - x_{i-\frac{1}{2}}}{\Delta x_i} - \tilde{x}_i \right) \right) \right). \quad (24)$$

The parameter α in Eq. (24) is specified as

$$\alpha = \begin{cases} 1 & \text{if } C_{i-1} < C_{i+1}, \\ -1 & \text{if } C_{i-1} > C_{i+1}. \end{cases} \quad (25)$$

Parameter β is chosen to be 3.5 to control the sharpness of the variation of the function. To determine the jump center of the hyperbolic tangent function, another parameter \tilde{x}_i is used and is calculated as follows:

$$\begin{aligned}
C_i &= \frac{1}{\Delta x_i} \int_{x_{i-1/2}}^{x_{i+1/2}} \chi_{x, \tilde{x}_i}(x) dx \\
&= \frac{1}{\Delta x} \int_{x_{i-1/2}}^{x_{i+1/2}} \frac{1}{2} \left(1 + \alpha \tanh \left(\beta \left(\frac{x - x_{i-1/2}}{\Delta x} - \tilde{x}_i \right) \right) \right) dx
\end{aligned} \tag{26}$$

with

$$\tilde{x}_i = \frac{1}{2\beta} \ln \left(\frac{a_3^2 - a_1 a_3}{a_1 a_3 - 1} \right), \tag{27}$$

where $a_1 = \exp\left(\frac{\beta}{\alpha}(2C_i - 1)\right)$ and $a_3 \equiv \exp(\beta)$. Following this, we integrate THINC and WLIC schemes to one scheme, THINC/WLIC, by substituting $\chi_{i,j}(x, y)$ derived in Eq. (20) into Eq. (16) to calculate the numerical flux $F_{x,i+1/2,j}$

$$\begin{aligned}
F_{x,i+1/2,j} &= - \int_{y_{i,j-1/2}}^{y_{i,j+1/2}} \int_{x_{i+1/2,j}}^{x_{i+1/2,j} - u_{i+1/2,j}\Delta t} \chi_{is,j}(x, y) dx dy \\
&= - \int_{y_{i,j-1/2}}^{y_{i,j+1/2}} \int_{x_{i+1/2,j}}^{x_{i+1/2,j} - u_{i+1/2,j}\Delta t} \omega_{x,is,j} \chi_{x,is,j} dx dy
\end{aligned} \tag{28}$$

$$\begin{aligned}
&- \int_{y_{i,j-1/2}}^{y_{i,j+1/2}} \int_{x_{i+1/2,j}}^{x_{i+1/2,j} - u_{i+1/2,j}\Delta t} \omega_{y,is,j} \chi_{y,is,j} dx dy, \\
&\equiv F_{x,x,i+1/2,j}(\omega_{x,is,j}, \chi_{x,is,j}) + F_{x,y,i+1/2,j}(\omega_{y,is,j}, \chi_{y,is,j}).
\end{aligned} \tag{29}$$

The numerical flux $F_{x,i+1/2,j}$ in Eq. (28) contains two terms, $F_{x,x,i+1/2,j}$ and $F_{x,y,i+1/2,j}$, which can be calculated using the THINC scheme in order to have less oscillation and smearing in the fluid fraction function solution.

$$\begin{aligned}
F_{x,x,i+1/2,j} &= F_{x,x,i+1/2} = - \int_{x_{i+1/2}}^{x_{i+1/2} - u_{i+1/2}\Delta t} \omega_{x,is} \chi_{x,is} dx \\
&= - \int_{x_{i+1/2}}^{x_{i+1/2} - u_{i+1/2}\Delta t} \frac{\omega_{x,is}}{2} \left(1 + \alpha \tanh \left(\beta \left(\frac{x - x_{is-1/2}}{\Delta x} - \tilde{x}_{is} \right) \right) \right) dx \\
&= - \frac{\omega_{x,is}}{2} \left[x + \frac{\alpha \Delta x}{\beta} \ln \left(\cosh \left(\beta \left(\frac{x - x_{is-1/2}}{\Delta x} \right) - \tilde{x}_{is} \right) \right) \right]_{x_{i+1/2}}^{x_{i+1/2} - u_{i+1/2}\Delta t}
\end{aligned} \tag{30}$$

and

$$F_{x,y,i+1/2,j} = \omega_{y,is,j} C_{is,j} u_{x,i+1/2,j} \Delta t. \tag{31}$$

2.4. Coupled VOF function with signed distance function

The present VOF method introduces a new LS field ϕ , and the interface is also defined by the zero LS $\phi = 0$. In standard CLSVOF methods, both LS and VOF advection equations need to be solved [38]; in the present VOF method, however, only the VOF advection equation (Eq. (12)) is solved.

After the volume fraction is advected (i.e. Eq. (3)), we convert the volume fraction into updated distance function ϕ^{n+1} at interfacial cells ($0 < C < 1$). Two steps are required for the converting procedure:

STEP 1

Assume that the interface is defined at the contour $C = 0.5$, and use the advected VOF fraction function to assign an initial value to the LS function:

$$\phi_0 = 2C - 1. \quad (32)$$

ϕ_0 is positive in the liquid and negative in the gas. Then, the interface defined by the $C = 0.5$ contour is converted into the zero LS contour $\phi_0 = 0$.

STEP 2

Following this, the following re-initialization equation is solved to ensure that the LS value ϕ_0 is a distance function, so that the interface normals in Eq. (20) and the surface tension terms in Eq. (2) can be calculated [50]

$$\phi_\tau = \bar{S}(\phi_0)(1 - |\nabla\phi|) + \lambda\delta(\phi)|\nabla\phi|, \quad (33)$$

where τ is the artificial time step and $\bar{S}(\phi_0)$ is the smoothed sign function:

$$\bar{S}(\phi_0) = 2(\mathcal{H}(\phi_0) - 0.5). \quad (34)$$

The parameter λ in Eq. (33) is expressed as

$$\lambda = - \frac{\int_{\Omega} \delta(\phi) (\bar{S}(\phi_0)(1 - |\nabla\phi|)) d\Omega}{\int_{\Omega} \delta^2(\phi) |\nabla\phi| d\Omega}. \quad (35)$$

The above re-initialization equation is discretized by the fifth-order weighted essentially non-oscillatory (WENO5) scheme in space by Jiang and Peng [51], and is discretized by the third-order total variation diminishing Runge–Kutta (TVD-RK3) scheme in time by Shu [52].

3. Solution procedure for the proposed VOF method and two-phase flow algorithm

The Navier–Stokes equations are discretized on staggered grids, in which the pressure p is defined at cell centers and the velocity vector \mathbf{u} is located at centers of cell faces. The detailed solution procedure in this study is summarized as follows:

STEP 1: Set the initial condition for velocity \mathbf{u} and volume fraction function ($C = 1$ in the liquid and $C = 0$ in the gas).

STEP 2: Calculate the LS function by $\phi_0 = 2C - 1$, and initialize the LS function by solving Eq. (33) in order to obtain the signed distance function for ϕ .

STEP 3: Calculate the curvature in Eq. (5) by using the signed distance function ϕ .

STEP 4: Advect the VOF function by using the modified THINC/WLIC scheme introduced in Section 2.3.

STEP 5: Approximate the diffusive terms in the momentum equation by using the second-order accurate central difference scheme. Approximate the convective terms by using the following second-order upwinding scheme:

$$u \frac{\partial u}{\partial x} = \frac{1}{2\Delta x} (u^+ (3u_{i,j,k} - 4u_{i-1,j,k} + u_{i-2,j,k}) + u^- (-u_{i+2,j,k} + 4u_{i+1,j,k} - 3u_{i,j,k})), \quad (36)$$

where $u^+ = \frac{1}{2}(u_{i,j} + |u_{i,j}|)$ and $u^- = \frac{1}{2}(u_{i,j} - |u_{i,j}|)$.

STEP 6: Calculate $\mathbf{u}^{n+1/2}$ by the second-order explicit Adams–Bashforth scheme

$$\frac{\mathbf{u}^{n+1/2} - \mathbf{u}^n}{\Delta t} + \left(\frac{3}{2} \mathbf{A}^n - \frac{1}{2} \mathbf{A}^{n-1} \right) = 0, \quad (37)$$

where $\mathbf{A}^n = \mathbf{u}^n \cdot \nabla \mathbf{u}^n - \frac{1}{\rho^n} \nabla \cdot [\mu^n (\nabla \mathbf{u}^n + (\nabla \mathbf{u}^n)^T)] - \frac{\mathbf{F}_B}{\rho}$.

STEP 7: Define physical properties $\rho(C)$ and $\mu(C)$ according to the VOF function C^{n+1} .

STEP 8: Solve the Poisson equation $\nabla \cdot (\frac{1}{\rho^{n+1}} \nabla p^{n+1}) = \frac{1}{\Delta t} \nabla \cdot \mathbf{u}^{n+1/2}$ by the point-successive over-relaxation (SOR) method for the pressure field p^{n+1} .

STEP 9: Solve $\frac{\mathbf{u}^{n+1} - \mathbf{u}^{n+1/2}}{\Delta t} = -\frac{1}{\rho^{n+1}} \nabla p^{n+1}$ for velocity \mathbf{u}^{n+1} .

STEP 10: Repeat Steps 2–9 for one time loop.

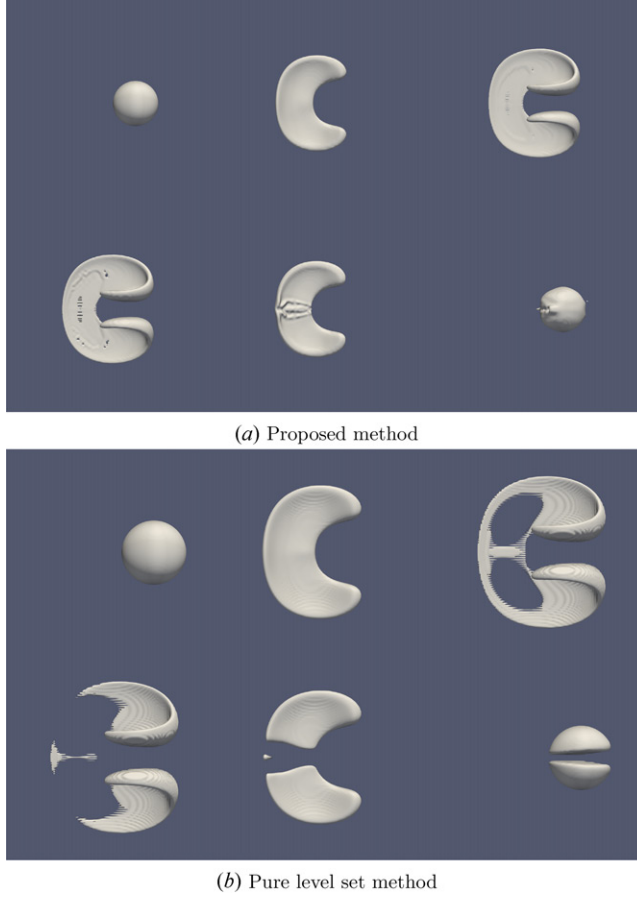


Figure 1. Snapshots of the predicted interfaces of the three-dimensional vortex deforming problem predicted in grids 128^3 . From top to bottom, from left to right, $t = 0, 0.6, 1.2, 1.8, 2.4, 3.0$. (a) Proposed method. (b) Pure level set method.

4. Numerical results

To demonstrate that the proposed VOF and LS [50] advection algorithm has the ability to preserve mass and ensure accuracy, the vortex deforming problem is considered first. Note that the advection terms for the LS method are discretized by the WENO scheme [51]. Following this, three bubble/droplet problems which take surface tension force into consideration are investigated to justify the proposed VOF method and incompressible two-phase flow solver. The loss of mass under investigation involves VOF function given below

$$\hat{\varepsilon}_M = \frac{|M_t - M_0|}{M_0} \times 100\%, \quad (38)$$

where $M_0 = \int_{\Omega} C(t=0) d\Omega$ and $M_t = \int_{\Omega} C(t) d\Omega$ are the mass at the beginning and at the end of the computation, respectively.

4.1. Vortex deforming problem

One method to assess the accuracy of interface capturing methods is to apply it to the simulation of a liquid sphere in a single vortex flow field [30]. The test is particularly challenging to interface resolving methods when the resulting liquid ligament becomes thin compared with the grid size.

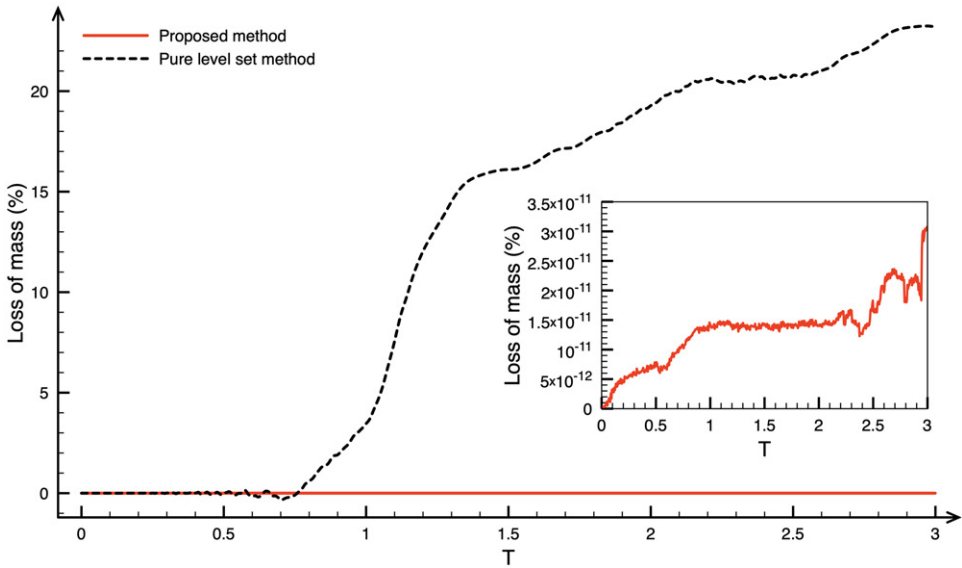
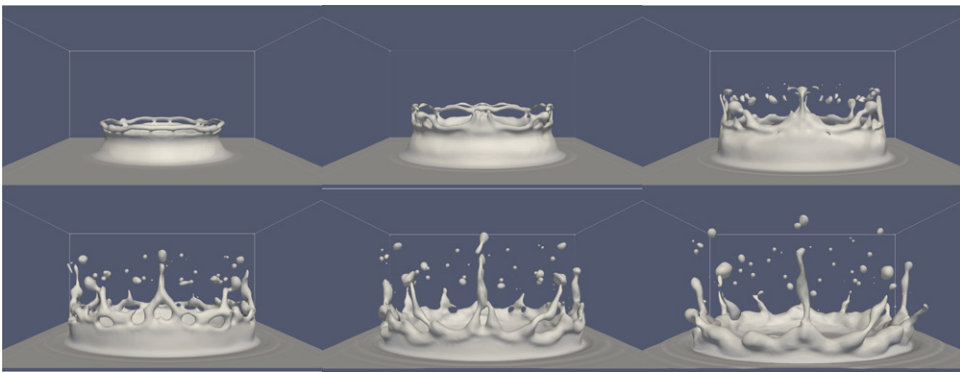
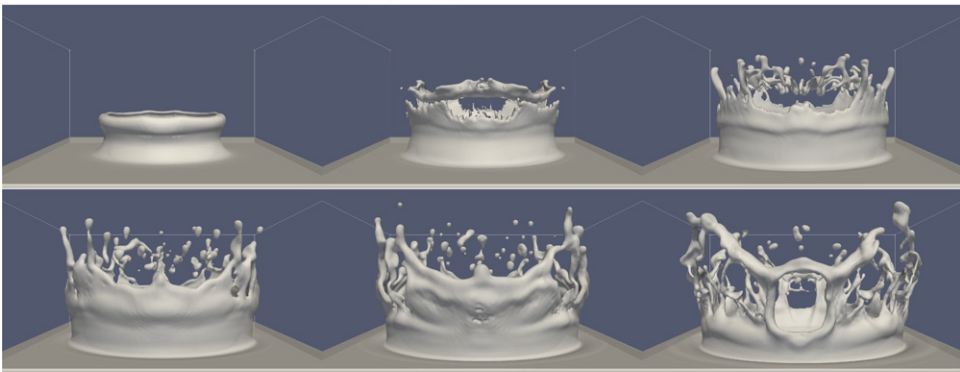


Figure 2. Predicted mass loss of the three-dimensional vortex deforming problem. (a) Proposed method. (b) Pure level set method.



(a) Proposed method



(b) Pure level set method

Figure 3. Snapshots of the predicted interfaces of the milk crown problem predicted in grids $210 \times 210 \times 105$.

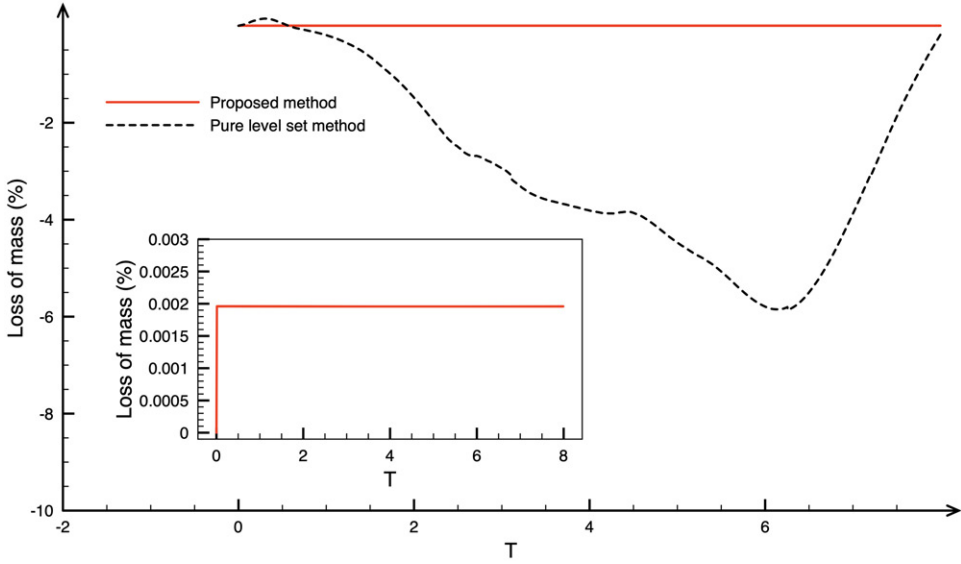


Figure 4. Predicted mass loss of the milk crown problem. (a) Proposed method. (b) Pure level set method.

The current VOF method is evaluated using this case and the results are compared with those by LS results.

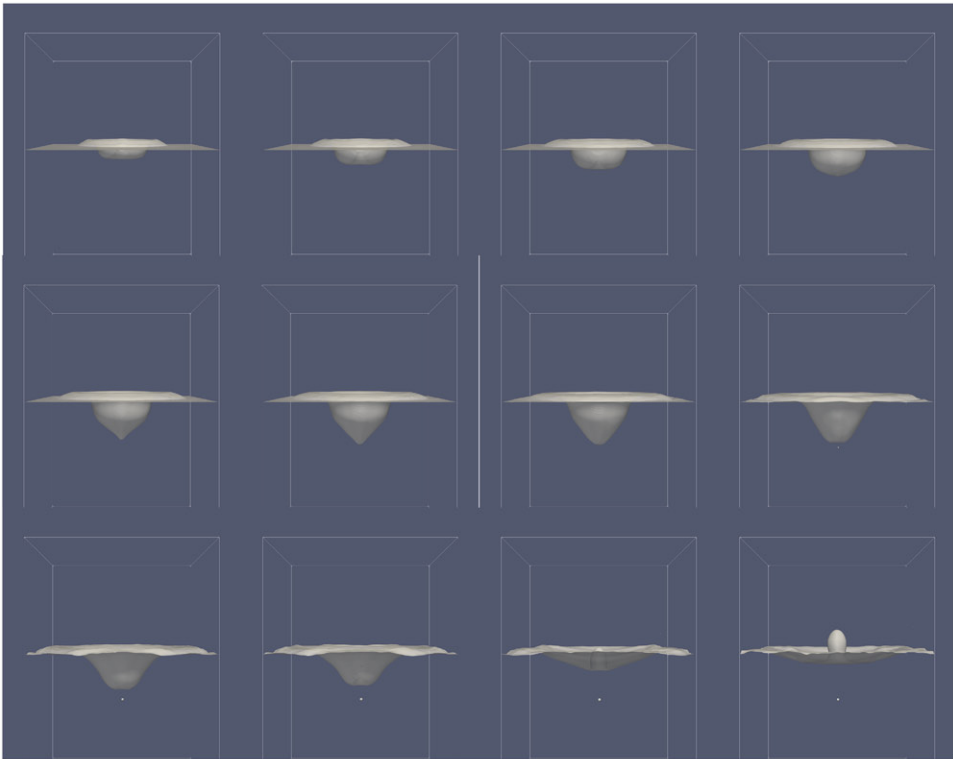
A sphere (radius $r=0.15$) is initially located in a unit cube with its center placed at $(0.35, 0.35, 0.35)$. The velocity field is given by its components as

$$\begin{aligned}
 u(x, y, z, t) &= 2 \sin(\pi x)^2 \sin(2\pi y) \sin(2\pi z) \cos\left(\frac{\pi t}{T}\right), \\
 v(x, y, z, t) &= -\sin(2\pi x) \sin(\pi y)^2 \sin(2\pi z) \cos\left(\frac{\pi t}{T}\right), \\
 w(x, y, z, t) &= -\sin(2\pi x) \sin(2\pi y) \sin(\pi z)^2 \cos\left(\frac{\pi t}{T}\right),
 \end{aligned} \tag{39}$$

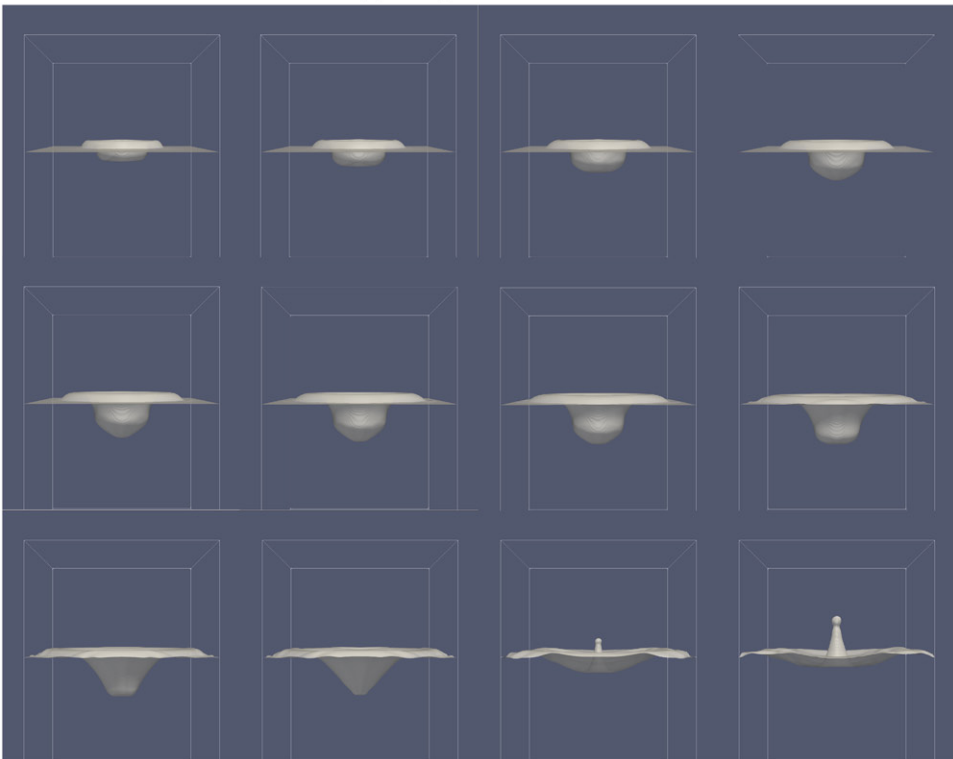
where t denotes time. $T=3.0$ is the time required for a full rotation. **Figure 1** shows the predicted interfaces in 128^3 grids using the proposed method and a pure LS method at several time instants during the rotation. It can be seen that the proposed VOF method provides more accurate results than the LS method. **Figure 2** presents the mass error calculated from Eq. (38) for the proposed VOF method and the LS method. The proposed VOF method conserves mass quite well, while significant mass loss is found in the LS method.

4.2. Droplet impacting a thin liquid layer (milk crown)

We simulated droplet impacting a thin liquid layer by using the proposed VOF method. A set of parameters were used: the densities $\rho_L = 1,000 \text{ kg/m}^3$, $\rho_G = 1.25 \text{ kg/m}^3$, the viscosity coefficients $\mu_L = 1.7 \times 10^{-3} \text{ Pa s}$, $\mu_G = 1.0 \times 10^{-6} \text{ Pa s}$, the surface tension coefficient $\sigma = 5 \times 10^{-2} \text{ N/m}$, the gravity 9.8 m/s^2 , the initial droplet diameter $D = 5.33 \text{ mm}$, and the depth of liquid layer 1 mm . We simulated for Weber numbers ($We = \frac{\rho_L U^2 D}{\sigma} = 426$), where $U = 2 \text{ m/s}$ is droplet impact speed [53]. **Figure 3** shows the numerical results. The tiny droplet at the tip of the milk crown, which is called the spike, and the generation of spear-type splash, which is the secondary splash formed after the milk crown, are realized well as seen



(a) Proposed method



(b) Pure level set method

Figure 5. Snapshots of the predicted interfaces of the droplet impacting a deep liquid pool problem predicted in grids $175 \times 175 \times 245$.

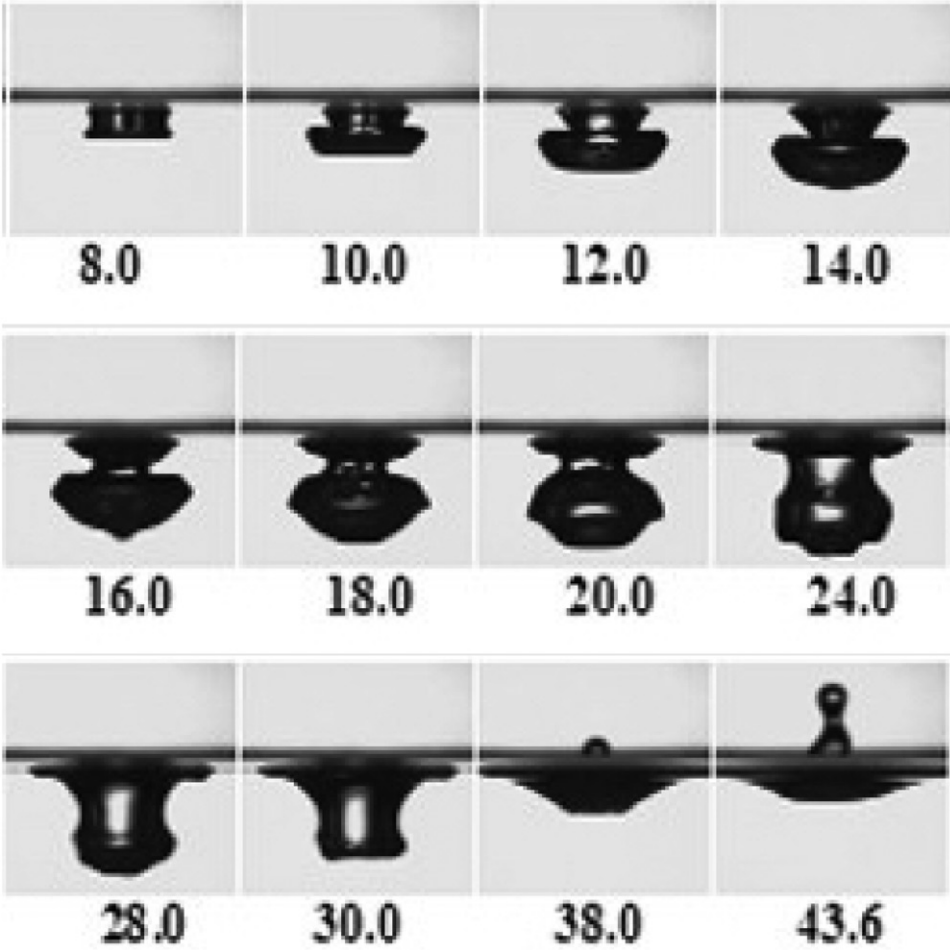


Figure 6. Experimental snapshots of the problem of droplet impact into deep liquid pool. (a) Proposed method. (b) Pure level set method.

in the simulation. Mass conservation results of the proposed VOF and LS methods are also compared as shown in Figure 4.

4.3. Droplet impacting into a deep liquid pool

The droplet impacting into a deep liquid pool is experimentally investigated in Ref. [54]. The impacting velocity is theoretically derived from Newton's law as follows:

$$V = V_T \tanh \left[\left(\frac{g}{V_T} \right) t + \tanh^{-1} \left(\frac{V_0}{V_T} \right) \right], \quad (40)$$

where g is the acceleration of gravity, and t , V_0 , and V_T are the falling time, initial velocity after pinch-off, and the terminal velocity of a drop obtained from the empirical formula [55]. Figure 5 shows the evolution of impacting craters due to drops falling with velocity $V = 0.964$ m/s and diameter $d = 5.65$ mm. The Weber number $We = \frac{\rho V^2 d}{\sigma} = 77$ and Froude number $Fr = \frac{V^2}{gd} = 17$ are used, where ρ and σ are density and surface tension of the drop, respectively. Figure 6 shows

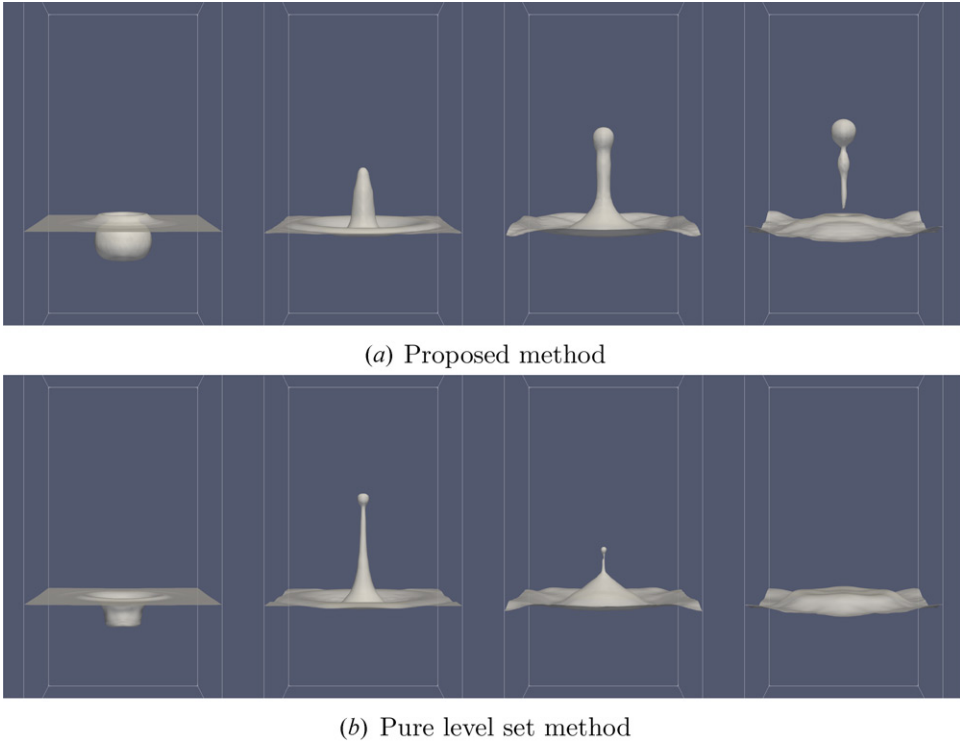


Figure 7. Snapshots of the predicted interfaces of the bubble burst at the free surface predicted in grids $90 \times 90 \times 180$. From left to right, $t = 0.5, 1.0, 1.5, 2.0$.

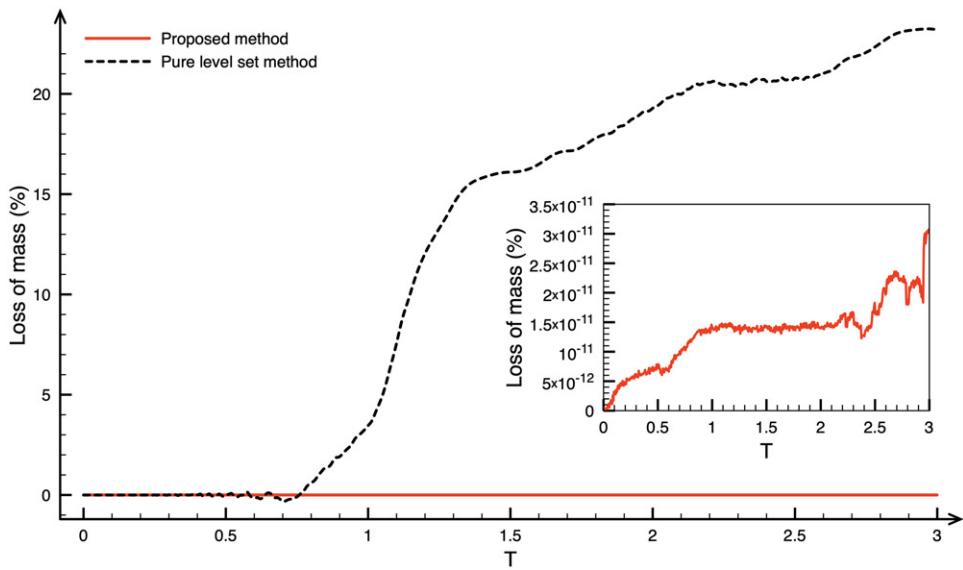


Figure 8. Predicted mass loss of the bubble burst at the free surface problem.

the experiment results [54]. The LS and VOF solutions agree well with experiment results without deterioration of accuracy.

4.4. Bubble bursting at a free surface

A three-dimensional spherical bubble rising in water is considered in Ref. [56]. This rising bubble is initially placed at $(x, y, z) = (0, 0, -3.2)$ in a box of $[-2, 2] \times [-2, 2] \times [-6, 6]$. No slip boundary conditions are imposed on all walls of the box. The computational grid is $90 \times 90 \times 180$ in this study. The dimensionless Reynolds and Weber numbers are $Re = 474$, $We = 1$, respectively. Froude number is defined as $Fr = \frac{U}{\sqrt{gR}} = 0.64$, where R is the bubble radius. Note that high viscosity and density ratios of water to air as 0.01 and 0.001 are adopted, respectively. Four snapshots of the numerical solutions are present in Figure 7 at $t = 0.5$, $t = 1.0$, $t = 1.5$, and $t = 2.0$. In Figure 7a, b, the present simulation by the VOF method is shown together with that from the LS method. The proposed VOF method shows the pinch-off process of liquid jets and the generation of liquid droplets that follows. The mass error as defined in Eq. (38) is almost zero by using the proposed VOF method as Figure 8.

5. Concluding remarks

This article presents a VOF model for simulation of bubble/droplet two-phase flows. The proposed VOF method conserves mass well and can easily estimate interface normals from the LS function. The LS function is a continuous signed distance function, and is expressed by solving the re-initialization equation. The milk crown, droplet impacting on a deep liquid pool, and bubble bursting on a free surface problems are investigated. The numerical results agree well with the experimental results for the droplet impacting on a deep liquid pool problem. In addition, this model can effectively simulate problems with strong topological changes such as break up and merging even when surface tension force needs to be considered.

Funding

This work was supported by the National Key Research and Development Program of China under Grant 2018YFC1508100; the National Key Research and Development Program of China 4th sub-topic under Grant 2018YFC1508104; the National Natural Science Foundation of China under Grant 91547211, 51579216; the Sichuan Provincial Natural Science Foundation of China under Grant 2019YJ0118; and Innovation spark project under Grant SCUH0049.

References

- [1] H. Hwang, and G. Son, "A level-set method for the direct numerical simulation of particle motion in droplet evaporation," *Numer. Heat Transf. B*, vol. 68, no. 6, pp. 479–494, 2015. DOI: [10.1080/10407790.2015.1052309](https://doi.org/10.1080/10407790.2015.1052309).
- [2] P. Datta, A. Chakravarty, K. Ghosh, A. Mukhopadhyay, and S. Sen, "Modeling aspects of vapor bubble condensation in subcooled liquid using the VOF approach," *Numer. Heat Transf. A*, vol. 72, no. 3, pp. 236–254, 2017. DOI: [10.1080/10407782.2017.1372673](https://doi.org/10.1080/10407782.2017.1372673).
- [3] X. Huang, L. He, X. Luo, D. Yang, K. Shi, and H. Yan, "Breakup mode transformation of leaky dielectric droplet under direct current electric field," *Int. J. Multiphas. Flow*, vol. 96, pp. 123–133, 2017. DOI: [10.1016/j.ijmultiphaseflow.2017.07.007](https://doi.org/10.1016/j.ijmultiphaseflow.2017.07.007).
- [4] D. Khojasteh, A. Bordbar, R. Kamali, and M. Marengo, "Curvature effect on droplet impacting onto hydrophobic and superhydrophobic spheres," *Int. J. Comput. Fluid D*, vol. 31, no. 6–8, pp. 310–323, 2017. DOI: [10.1080/10618562.2017.1349312](https://doi.org/10.1080/10618562.2017.1349312).
- [5] G. Son, and V. K. Dhir, "A level set Method for analysis of film boiling on an immersed solid surface," *Numer. Heat Transf. B*, vol. 52, no. 2, pp. 153–177, 2007. DOI: [10.1080/10407790701347720](https://doi.org/10.1080/10407790701347720).

- [6] K. Yokoi, M. Furuichi, and M. Sakai, "An efficient multi-dimensional implementation of VSIAM3 and its applications to free surface flows," *Phys. Fluids*, vol. 29, no. 12, pp. 121611, 2017. DOI: [10.1063/1.4996183](https://doi.org/10.1063/1.4996183).
- [7] C. Shao, K. Luo, Y. Yang, and J. Fan, "Detailed numerical simulation of swirling primary atomization using a mass conservative level set method," *Int. J. Multiphas. Flow*, vol. 89, pp. 57–68, 2017. DOI: [10.1016/j.ijmultiphaseflow.2016.10.010](https://doi.org/10.1016/j.ijmultiphaseflow.2016.10.010).
- [8] B. M. Ningegowda, and B. Premachandran, "A coupled level set and volume of fluid method with multi-directional advection algorithms for two-phase flows with and without phase change," *Int. J. Heat Mass Transf.*, vol. 79, pp. 532–550, 2014. DOI: [10.1016/j.ijheatmasstransfer.2014.08.039](https://doi.org/10.1016/j.ijheatmasstransfer.2014.08.039).
- [9] M. Haghshenas, J. A. Wilson, and R. Kumar, "Algebraic coupled level set-volume of fluid method for surface tension dominant two-phase flows," *Int. J. Multiphas. Flow*, vol. 90, pp. 13–28, 2017. DOI: [10.1016/j.ijmultiphaseflow.2016.12.002](https://doi.org/10.1016/j.ijmultiphaseflow.2016.12.002).
- [10] S. O. Unverdi, and G. Tryggvason, "A front tracking method for viscous, incompressible, multi fluid flows," *J. Comput. Phys.*, vol. 100, pp. 25–37, 1992. DOI: [10.1016/0021-9991\(92\)90307-K](https://doi.org/10.1016/0021-9991(92)90307-K).
- [11] J. Han, and G. Tryggvason, "Secondary breakup of axisymmetric liquid drops. I. Acceleration by a constant body force," *Phys. Fluids*, vol. 11, pp. 3650–3718, 1999. DOI: [10.1063/1.870229](https://doi.org/10.1063/1.870229).
- [12] W. Yang, M. Jia, Z. Che, K. Sun, and T. Wang, "Transitions of deformation to bag breakup and bag to bag-stamen breakup for droplets subjected to a continuous gas flow," *Int. J. Heat Mass Transf.*, vol. 111, pp. 884–894, 2017. DOI: [10.1016/j.ijheatmasstransfer.2017.04.012](https://doi.org/10.1016/j.ijheatmasstransfer.2017.04.012).
- [13] C. W. Hirt, and B. D. Nichols, "Volume of fluid (VOF) method for the dynamics of free boundaries," *J. Comput. Phys.*, vol. 39, no. 1, pp. 201–225, 1981. DOI: [10.1016/0021-9991\(81\)90145-5](https://doi.org/10.1016/0021-9991(81)90145-5).
- [14] Y. Y. Tsui, and S. W. Lin, "A VOF-based conservative interpolation scheme for interface tracking (CISIT) of two-fluid flows," *Numer. Heat Transf. B*, vol. 63, no. 4, pp. 263–283, 2013. DOI: [10.1080/10407790.2013.756251](https://doi.org/10.1080/10407790.2013.756251).
- [15] A. Zhang, Y. Wang, D. Sun, S. Yu, B. Yu, and Y. Li, "Development of a VOF + LS + SPP method based on FLUENT for simulating bubble behaviors in the electric field," *Numer. Heat Transf. B*, vol. 71, no. 2, pp. 186–201, 2017. DOI: [10.1080/10407790.2016.1265308](https://doi.org/10.1080/10407790.2016.1265308).
- [16] P. Rauschenberger *et al.*, "Comparative assessment of volume-of-fluid and level-set methods by relevance to dendritic ice growth in supercooled water," *Comput. Fluids*, vol. 79, pp. 44–52, 2013. DOI: [10.1016/j.compfluid.2013.03.010](https://doi.org/10.1016/j.compfluid.2013.03.010).
- [17] Z. Ye, X. Zhao, and Z. Deng, "Numerical investigation of the gate motion effect on a dam break flow," *J. Mar. Sci. Technol.*, vol. 21, no. 4, pp. 579–591, 2016. DOI: [10.1007/s00773-016-0374-1](https://doi.org/10.1007/s00773-016-0374-1).
- [18] D. Hui, G. Y. Zhang, D. P. Yua, Z. Sun, and Z. Zong, "Numerical study of advection schemes for interface-capturing using gradient smoothing method," *Numer. Heat Transf. B*, vol. 73, no. 4, pp. 242–261, 2018. DOI: [10.1080/10407790.2018.1462005](https://doi.org/10.1080/10407790.2018.1462005).
- [19] S. Osher, and J. A. Sethian, "Fronts propagating with curvature dependent speed: algorithms based on Hamilton–Jacobi formulations," *J. Comput. Phys.*, vol. 79, no. 1, pp. 12–49, 1988. DOI: [10.1016/0021-9991\(88\)90002-2](https://doi.org/10.1016/0021-9991(88)90002-2).
- [20] Y. F. Yap, J. C. Chai, T. N. Wong, K. C. Toh, and H. Y. Zhang, "A global mass correction scheme for the level-set method," *Numer. Heat Transf. B*, vol. 50, no. 5, pp. 455–472, 2006. DOI: [10.1080/10407790600646958](https://doi.org/10.1080/10407790600646958).
- [21] L. Zhao, J. Mao, X. Bai, X. Liu, T. Li, and J. J. R. Williams, "Finite element implementation of an improved conservative level set method for two phase flow," *Comput. Fluids*, vol. 100, pp. 138–154, 2014. DOI: [10.1016/j.compfluid.2014.04.027](https://doi.org/10.1016/j.compfluid.2014.04.027).
- [22] E. Schillaci, L. Jofre, N. Balcázar, O. Lehmkuhl, and A. Oliva, "A level-set aided single-phase model for the numerical simulation of free-surface flow on unstructured meshes," *Comput. Fluids*, vol. 140, pp. 97–110, 2016. DOI: [10.1016/j.compfluid.2016.09.014](https://doi.org/10.1016/j.compfluid.2016.09.014).
- [23] F. Zhang, X. Zhang, K. Y. Sze, Y. P. Lian, and Y. Liu, "Incompressible material point method for free surface flow," *J. Comput. Phys.*, vol. 330, pp. 92–110, 2017. DOI: [10.1016/j.jcp.2016.10.064](https://doi.org/10.1016/j.jcp.2016.10.064).
- [24] Y. F. Yap, H. Y. Li, J. Lou, L. S. Pan, and Z. Shang, "Numerical modeling of three-phase flow with phase change using the level-set method," *Int. J. Heat Mass Transf.*, vol. 115, pp. 730–740, 2017. DOI: [10.1016/j.ijheatmasstransfer.2017.08.076](https://doi.org/10.1016/j.ijheatmasstransfer.2017.08.076).
- [25] M. Sussman, P. Smereka, and S. Osher, "A level set approach for computing solutions to incompressible two-phase flow," *J. Comput. Phys.*, vol. 114, no. 1, pp. 146–159, 1994. DOI: [10.1006/jcph.1994.1155](https://doi.org/10.1006/jcph.1994.1155).
- [26] K. Yokoi, "A variational approach to multi-phase motion of gas, liquid and solid based on the level set method," *Comput. Phys. Commun.*, vol. 180, no. 7, pp. 1145–1149, 2009. DOI: [10.1016/j.cpc.2009.01.022](https://doi.org/10.1016/j.cpc.2009.01.022).
- [27] J. Yang, and F. Stern, "Sharp interface immersed-boundary/level-set method for wave-body interactions," *J. Comput. Phys.*, vol. 228, no. 17, pp. 6590–6616, 2009. DOI: [10.1016/j.jcp.2009.05.047](https://doi.org/10.1016/j.jcp.2009.05.047).
- [28] A. Zandian, W. A. Sirignano, and F. Hussain, "Planar liquid jet: early deformation and atomization cascades," *Phys. Fluids*, vol. 29, no. 6, pp. 062109, 2017. DOI: [10.1063/1.4986790](https://doi.org/10.1063/1.4986790).

- [29] C. X. Shao, K. Luo, S. Chen, and J. R. Fan, “A mass conserving level set method for detailed numerical simulation of liquid atomization,” *J. Comput. Phys.*, vol. 298, pp. 495–519, 2015. DOI: [10.1016/j.jcp.2015.06.009](https://doi.org/10.1016/j.jcp.2015.06.009).
- [30] C. H. Yu, and T. W. H. Sheu, “Simulation of incompressible free surface flow using the volume preserving level set method,” *Commun. Comput. Phys.*, vol. 18, no. 4, pp. 931–956, 2015. DOI: [10.4208/cicp.081214.240515s](https://doi.org/10.4208/cicp.081214.240515s).
- [31] J. Lee, and G. Son, “A level-set method for ultrasound-driven bubble motion with a phase change,” *Numer. Heat Transf. A*, vol. 71, no. 9, pp. 928–943, 2017. DOI: [10.1080/10407782.2017.1326786](https://doi.org/10.1080/10407782.2017.1326786).
- [32] M. Griebel, and M. Klitz, “Simulation of droplet impact with dynamic contact angle boundary conditions,” in *Singular Phenomena and Scaling in Mathematical Models*, M. Griebel, Ed. Springer International Publishing, 2014, pp. 297–325. DOI: https://doi.org/10.1007/978-3-319-00786-1_13
- [33] F. Xiao, Y. Honma, and T. Kono, “A simple algebraic interface capturing scheme using hyperbolic tangent function,” *Int. J. Numer. Meth. Fluids*, vol. 48, no. 9, pp. 1023–1040, 2005. DOI: [10.1002/fld.975](https://doi.org/10.1002/fld.975).
- [34] W. F. Noh, and P. Woodward, “SLIC (simple line interface calculation),” Proceedings of the Fifth International Conference on Numerical Methods in Fluid Dynamics, 5th, Enschede, Netherlands, June 28–July 2. Berlin and New York: Springer-Verlag, 1976, pp. 330–340. DOI: [10.1007/3-540-08004-X_336](https://doi.org/10.1007/3-540-08004-X_336)
- [35] D. L. Youngs, “Time-dependent multi-material flow with large fluid distortion,” *Numer. Meth. Fluid Dyn.*, vol. 24, pp. 273–285, 1982.
- [36] Z. Cao, D. Sun, B. Yu, and J. Wei, “A coupled volume of fluid and level set method based on analytic PLIC for unstructured quadrilateral grids,” *Numer. Heat Transf. B*, vol. 73, no. 4, pp. 189–205, 2018. DOI: [10.1080/10407790.2018.1454758](https://doi.org/10.1080/10407790.2018.1454758).
- [37] K. Yokoi, “Efficient implementation of THINC scheme: a simple and practical smoothed VOF algorithm,” *J. Comput. Phys.*, vol. 226, no. 2, pp. 1985–2002, 2007. DOI: [10.1016/j.jcp.2007.06.020](https://doi.org/10.1016/j.jcp.2007.06.020).
- [38] M. Sussman, and E. G. Puckett, “A coupled level set and volume of fluid method for computing 3D and axisymmetric incompressible two-phase flows,” *J. Comput. Phys.*, vol. 162, no. 2, pp. 301–337, 2000. DOI: [10.1006/jcph.2000.6537](https://doi.org/10.1006/jcph.2000.6537).
- [39] G. Son, “Efficient implementation of a coupled level-set and volume-of-fluid method for three dimensional incompressible two-phase flows,” *Numer. Heat Transf. B*, vol. 43, no. 6, pp. 549–565, 2003. DOI: [10.1080/713836317](https://doi.org/10.1080/713836317).
- [40] K. Yokoi, “A practical numerical framework for free surface flows based on CLSVOF method, multi-moment methods and density-scaled CSF model: numerical simulations of droplet splashing,” *J. Comput. Phys.*, vol. 232, no. 1, pp. 252–271, 2013. DOI: [10.1016/j.jcp.2012.08.034](https://doi.org/10.1016/j.jcp.2012.08.034).
- [41] I. Chakraborty, G. Biswas, and P. S. Ghoshdastidar, “A coupled level-set and volume-of-fluid method for the buoyant rise of gas bubbles in liquids,” *Int. J. Heat Mass Transf.*, vol. 58, no. 1–2, pp. 240–259, 2013. DOI: [10.1016/j.jheatmasstransfer.2012.11.027](https://doi.org/10.1016/j.jheatmasstransfer.2012.11.027).
- [42] W. P. Hong, and Y. B. Wang, “A coupled level set and volume-of-fluid simulation for heat transfer of the double droplet impact on a spherical liquid film,” *Numer. Heat Transf. B*, vol. 71, no. 4, pp. 359–371, 2017. DOI: [10.1080/10407790.2017.1293960](https://doi.org/10.1080/10407790.2017.1293960).
- [43] Y. Y. Tsui, C. Y. Liu, and S. W. Lin, “Coupled level-set and volume-of-fluid method for two-phase flow calculations,” *Numer. Heat Transf. B*, vol. 71, no. 2, pp. 173–185, 2017. DOI: [10.1080/10407790.2016.1265311](https://doi.org/10.1080/10407790.2016.1265311).
- [44] O. Desjardins, V. Moureau, and H. Pitsch, “An accurate conservative level set/ghost fluid method for simulating turbulent atomization,” *J. Comput. Phys.*, vol. 227, no. 18, pp. 8395–8416, 2008. DOI: [10.1016/j.jcp.2008.05.027](https://doi.org/10.1016/j.jcp.2008.05.027).
- [45] D. L. Sun, and W. Q. Tao, “A coupled volume-of-fluid and level set (VOSET) method for computing incompressible two-phase flows,” *Int. J. Heat Mass Transf.*, vol. 53, no. 4, pp. 645–655, 2010. DOI: [10.1016/j.jheatmasstransfer.2009.10.030](https://doi.org/10.1016/j.jheatmasstransfer.2009.10.030).
- [46] T. Wang, H. Li, Y. Feng, and D. Shi, “A coupled volume-of-fluid and level set (VOSET) method on dynamically adaptive quadtree grids,” *Int. J. Heat Mass Transf.*, vol. 67, no. 4, pp. 70–73, 2013. DOI: [10.1016/j.jheatmasstransfer.2013.08.006](https://doi.org/10.1016/j.jheatmasstransfer.2013.08.006).
- [47] Z. Cao, D. Sun, B. Yu, and J. Wei, “A coupled volume-of-fluid and level set (VOSET) method based on remapping algorithm for unstructured triangular grids,” *Int. J. Heat Mass Transf.*, vol. 111, pp. 232–245, 2017. DOI: [10.1016/j.jheatmasstransfer.2017.03.096](https://doi.org/10.1016/j.jheatmasstransfer.2017.03.096).
- [48] J. U. Brackbill, D. B. Kothe, and C. Zemach, “Continuum method for modelling surface tension,” *J. Comput. Phys.*, vol. 100, no. 2, pp. 335–354, 1992. DOI: [10.1016/0021-9991\(92\)90240-Y](https://doi.org/10.1016/0021-9991(92)90240-Y).
- [49] K. Yokoi, “A density-scaled continuum surface force model within a balanced force formulation,” *J. Comput. Phys.*, vol. 278, pp. 221–228, 2014. DOI: [10.1016/j.jcp.2014.08.034](https://doi.org/10.1016/j.jcp.2014.08.034).
- [50] M. Sussman, and E. Fatemi, “An efficient, interface-preserving level set redistancing algorithm and its application to interfacial incompressible fluid flow,” *SIAM J. Sci. Comput.*, vol. 20, no. 4, pp. 1165–1191, 1999. DOI: [10.1137/S1064827596298245](https://doi.org/10.1137/S1064827596298245).

- [51] G. S. Jiang, and D. Peng, “Weighted ENO schemes for Hamilton–Jacobi equations,” *SIAM J. Sci. Comput.*, vol. 21, no. 6, pp. 2126–2143, 2000. DOI: [10.1137/S106482759732455X](https://doi.org/10.1137/S106482759732455X).
- [52] C. W. Shu, “Total-variation diminishing time discretizations,” *SIAM J. Sci. Stat. Comput.*, vol. 9, no. 6, pp. 1073–1984, 1988. DOI: [10.1137/0909073](https://doi.org/10.1137/0909073).
- [53] K. Yokoi, “A numerical method for free-surface flows and its application to droplet impact on a thin liquid layer,” *J. Sci. Comput.*, vol. 35, no. 2–3, pp. 372–396, 2008. DOI: [10.1007/s10915-008-9202-z](https://doi.org/10.1007/s10915-008-9202-z).
- [54] A. B. Wang, C. C. Kuan, and P. H. Tsai, “Do we understand the bubble formation by a single drop impacting upon liquid surface?” *Phys. Fluids*, vol. 25, no. 10, pp. 101702, 2013. DOI: [10.1063/1.4822483](https://doi.org/10.1063/1.4822483).
- [55] N. Dingle, and Y. Lee, “Terminal fallspeeds of raindrops,” *J. Appl. Meteorol.*, vol. 11, no. 5, pp. 877–879, 1972. DOI: [10.1175/1520-0450\(1972\)011 <0877:TFOR> 2.0.CO;2](https://doi.org/10.1175/1520-0450(1972)011%3C0877:TFOR%3E2.0.CO;2).
- [56] C. H. Yu, Z. T. Ye, T. W. H. Sheu, Y. T. Lin, and X. Z. Zhao, “An improved interface preserving level set method for simulating three dimensional rising bubble,” *Int. J. Heat Mass. Transf.*, vol. 103, pp. 753–772, 2016. vol. DOI: [10.1016/j.ijheatmasstransfer.2016.07.096](https://doi.org/10.1016/j.ijheatmasstransfer.2016.07.096).